P_t	dynamic payback period, year
Q	energy, kWh
q_{abs}	thermal flux, W/m^2
R	pressure drop factor
S	suppression factor
T	temperature, K
v	velocity, m/s
x	vapor quality
X_{tt}	Martinelli number

Abbreviation

Bo	boiling number
CAP	capacity
CER	CO_2 emission reduction
EFPC	evacuated flat-plate solar collector
FBM	the factor of bare module
HTF	heat transfer fluid
MRE	mean relative error
Nu	Nusselt number
PEC	cost function
Pr	Prandtl number
Re	Renold number

Subscripts

2p	two phases
a	ambient
abs	absorber plate
b	bottom plate
c	convection
cond	conductivity

ele	electricity
eq	equipment
f	fluid
g	vapor phase
gla	glass
grd	ground
in	inlet
l	liquid phase
nb	nucleate boiling
ng	natural gas
out	outlet
r	radiation
tb	absorber tube

Greek letter

α	absorptance
β_{CF}	factor of the contingency fees
γ	surface tension, N/m
δ	error
ε	emittance
λ	thermal conductivity, W/ (m•K)
μ	dynamic viscosity, Pa•s
ρ	density, kg/m3
σ	Stefan-Boltzmann constant
τ	transmittance

1. Introduction

Steam is a sort of important product in the industrial manufacturing process, such as metallurgical engineering [1], medical industry [2], food processing [3], and so on.

It is generally produced by fossil energy-based boilers [4], such as coal, natural gas, and so on. However, fossil energy will not only cause environmental problems that are contrary to the goal of "carbon neutrality", but also brings great exergy losses between chemical energy and thermal energy. Besides, as a kind of strategic reserve, fossil energy is not always available to all countries [5]. Therefore, using renewable energy (such as solar energy) to generate low-pressure process steam for industrial sectors is a more promising approach since it is copious globally and has a relatively higher efficiency to produce thermal energy than other renewable energy forms.

The technology of steam generation by solar energy has been studied worldwide [6] and most works are focused on the concentrating solar collectors, such as the parabolic trough solar collector [7] and so on. However, the concentrating solar collectors are disadvantageous as they can only use solar beam irradiance, thereby a tracking device is inevitable in the initial cost.

The non-concentration solar collectors (such as the flat plate solar collector [8], the evacuated tube solar collector [9], and so forth) are also widely used in solar energy utilization fields that can harvest both the beam and diffuse solar irradiance. It is featured as technology maturity, convenient installation, and low production cost [10]. Nevertheless, due to its great heat losses (thermal conduction, convection, and radiation), it is usually used for domestic hot water and space heating occasions ($<$ 100 °C) [11], but not qualified for the process steam generation (100 – 250 °C) [1]. If the heat loss problem of the non-concentrating solar collector can be solved properly, it will have executable thermal performance in steam generation applications and achieve better solar efficiency than the concentrating ones in the regions with a high proportion of diffuse solar irradiance.

The current research devoted to steam generation by non-concentrating solar collectors is mainly focusing on the various methods to impede its heat losses, thereby promoting its thermal performance and fitting the process steam generation applications. Inert gases (such as Ar and Kr) are used for reducing the energy losses of flat plate solar collector since it has a low thermal conduction coefficient. When they are used for the flat plate solar collector instead of the air interlayer, the energy losses can be reduced by as much as 20% [12]. If reduce its pressure, the heat conduction effect can be held back more obviously, thereby enhancing its thermal performance. The outdoor test indicated that the thermal efficiency has reached 60% under low-pressure Kr gas insulation in the flat plate solar collector [13].

As another type of non-concentrating solar collector, the evacuated tube solar collector adopts a vacuum environment to inhibit thermal conduction and convection, thus its operating temperature is more suitable for steam generation. For example, an experiment is conducted that uses the heat pipe evacuated tube solar collector for steam generation [14]. A steam drum is employed as the condensation section of the heat pipe evacuated tubes array that can achieve 130 °C under non-concentration solar irradiance. For further temperature and pressure elevation, the compound parabolic concentrator evacuated tube structure is explored for 200 °C steam generation [15]. Evacuated tube solar collector for high-temperature steam generation in the applications of steam cooking, boilers, laundry, etc are also studied [16]. In addition to steam generation, an evacuated tube collector is used for acetone vapor generation to drive an organic Rankine cycle [17].

Many advanced solar thermal conversion materials are also used for steam generation [18, 19], and they are generally categorized as metallic nanoparticles [20], porous carbon materials [21], and plasmonic absorbers [22]. Graphene oxide-based aerogels with carefully tailored absorption, thermal, and hydrophilic properties can enable efficient (≈83%) solar steam generation under one-sun illumination [23]. Activated carbon fiber felt is used to generate steam efficiently, and its solar conversion efficiency has reached 79.4 % under one sun illumination [24]. Ag nanostructures were made into thin films for efficient generation of steam and this novel material attains steam generation efficiency of 68.3% with the irradiation of natural sunlight [25]. However, these solar harvesting processes are conducted under normal pressure and these novel energy materials are usually aimed at the solar desalination and clean water production problem.

In line with the above literature review, the current solar collector used for steam generation usually needs an optical tracking device and the conventional non-concentrating solar collector generally has low efficiency due to the great heat loss. Given the high demand for process steam in the industrial sectors but usually modest solar resources in their located regions, steam generation based on the high-efficient non-concentrating solar collector is urgently needed. In this paper, a high-efficient evacuated flat plate solar collector (EFPC) used for direct steam generation is propounded. It adopts a high-vacuum environment to impede the thermal conductivity and thermal convection effect. Hence, the operating temperature and thermal efficiency can both be promoted to meet the requirement of direct steam generation. Using the non-concentrating EFPC for direct steam generation brings the following merits. Firstly, since the high-vacuum environment is adopted to inhibit thermal conduction and convection, the thermal radiant loss has become the main heat loss source of the evacuated flat plate solar collector. It is mainly caused by the high temperature of the absorber plate that emits thermal radiation to the ambient [26]. In the direct steam generation process, the operation temperature of the solar collector will maintain nearly constant accounts for the water phase change process. As a result of this merit, the thermal efficiency of the solar collector will also be improved due to the relatively low average operating temperature. Secondly, the steam is generated in the absorber pipes which leads to a boiling heat transfer process that usually possesses a high heat transfer coefficient. In the previous studies of evacuated flat plate solar collectors [27], the working fluid is the pressurization water to prevent evaporation. Hence, the heat transfer fluid (HTF) exchanges heat with absorber tubes by heat convection effect. With direct steam generation instead, boiling heat transfer occurs in the absorber tubes which will improve the heat transfer coefficient greatly, thereby improving the thermal efficiency of the solar collector. Thirdly, during the direct steam generation process, the latent heat of the water will be fully employed to absorb the solar energy. Owing to the thermodynamic properties of water, the flow rate of the whole solar field will be greatly reduced and water resources are saved. Furthermore, the power consumption of the pump will be saved which is significant in the large-scale solar fields. Fourthly, the EFPC can harvest both beam and diffuse solar irradiation. Compared with the concentrating solar collectors, this merit makes the system can be installed in regions that don’t have abundant solar resources (such as east China which has vast process steam requirements). Finally, owing to the low operating temperature, the organic fluid is usually adopted as HTF in the conventional non-concentrating solar collectors for the two-phase heat transfer process [28]. Through EFPC deployment, the water/steam can be used as HTF that is easily obtained, free of contamination, and cheap. Therefore, the materialization of direct steam generation-based EFPC has bilateral profits for both the steam generation process and solar harvesting process themselves.

To prove the feasibility and superiority of the direct steam generation with the non-concentrating solar collector, an evacuated flat plate solar plant for direct steam generation is investigated in this paper. The validated numerical models by experiment are employed to manifest its thermal performance in terms of the thermal efficiency, thermal loss distribution, and energy flow situation. Besides, the traditional non-concentrating solar collector is usually used for the building space heating projects but there exists the solar seasonal mismatch problem in these solar projects, i.e., the solar energy resource and the solar collectors themselves are not made fully used in the non-heating season since the lower heating demand than the heating season [29]. To solve this problem, a dual-mode EFPC system is also established to produce low-temperature hot water in the heating season for space heating and generate process steam in the non-heating season.

Therefore, the direct steam generation-based EFPC is fully explored in this paper from the perspective of the thermal performance, the internal energy flow, thermal losses, and the practical applications to solve the solar seasonal mismatch issue. The structure of this paper is organized as follows. First of all, the configuration of the direct steam generation-based EFPC system is described in Section 2. The detailed numerical models are stated for the main energy transfer process together with the experimental results and numerical model validation are also conducted in this section. Then, the results of direct steam generation EFPC and discussion are detailedly elucidated in Section 3. Next, the energetic, economic, and environmental performance of the dual-mode EFPC system is presented in Section 4 and the comparison with the state-of-art is also carried out. Finally, the main conclusions are drawn in Section 5. It is believed that this technology will bring much more benefits to the solar thermal utilization field and promise to be instrumental in the future decarbonization process.

2. Methodology

2.1 System description

As shown in Fig. 1 (a), the direct steam generation-based EFPC system is composed of several pieces of EFPC in series to increase the length of the circulation loop. Since the non-concentration solar flux is much less than the concentration solar collection scenarios (such as the parabolic trough solar collector with the solar concentration ratio over 50 [30]), the EFPC panel is designed with two inlets and outlets such that the working fluid will pass each panel twice in the circulation loop.

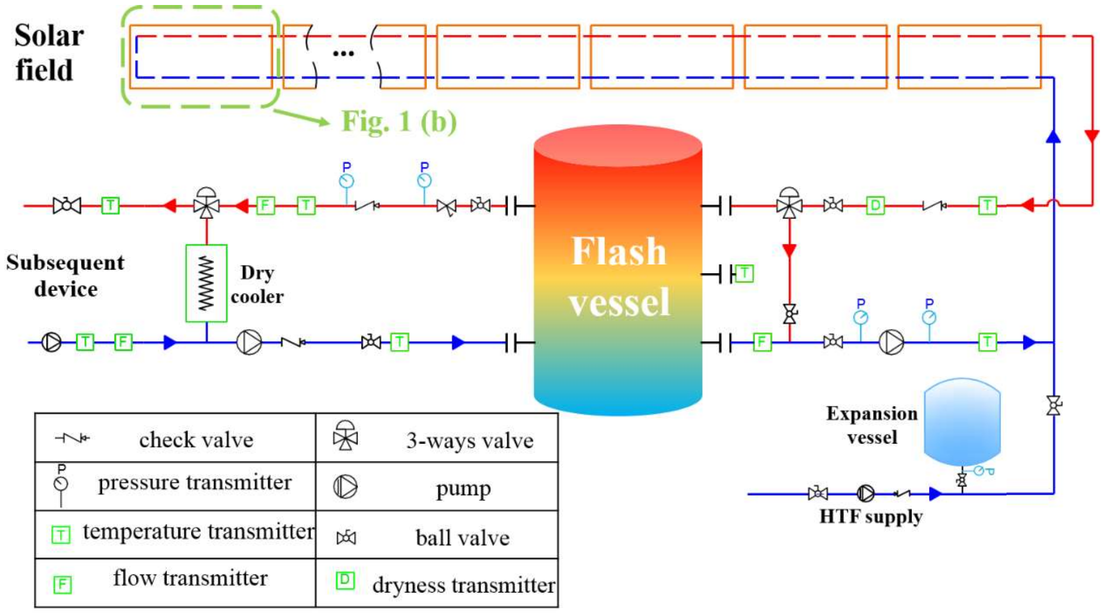

(a)

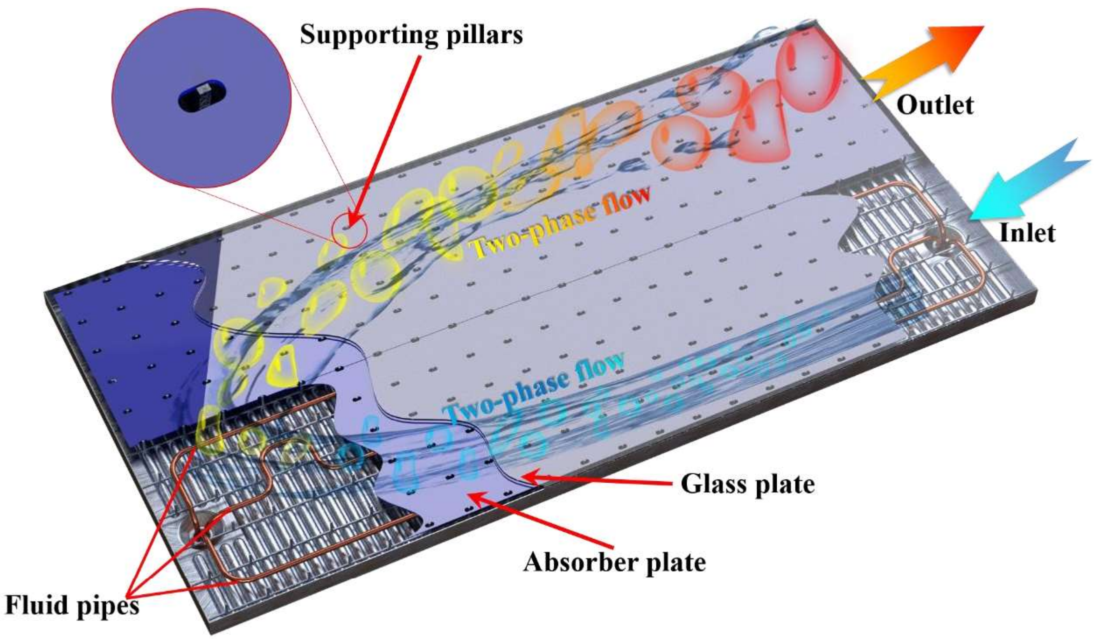

(b)

Fig. 1 The schematic structure of the direct steam generation EFPC system, (a) system configuration, and (b) detailed structure of single piece EFPC.

The structure of a single solar panel in the EFPC system is depicted in Fig. 1 (b), the inlet and outlet absorber tubes are both insulated in the vacuum environment. The two-phase flow inside the horizontal tubes will absorb the thermal energy from the absorber plate and increase its steam quality along the flow direction. The absorber plate is separated into two pieces to prevent the uneven temperature distribution on the absorber plate. A drimeter is adopted at the end of the return steam pipeline to check the dryness of the HTF. If the solar irradiance is weak which leads to a low steam quantity, the three-way value will change the pipe flow direction for HTF recirculation. The expansion vessel is used to adjust the working pressure of the pressurization HTF, thereby controlling the operating temperature of the whole solar plant. A pressurization pump and air vent channel will work synergistically to adjust the pressure of the whole solar plant. The flash vessel is used to store the HTF and supply energy to the subsequent device. The boiling heat transfer process in the EFPC will deteriorate if the solar irradiance is too strong and the flash vessel has reached its maximum storage capacity. The dry cooler can be used to dissipate the stored energy to prevent overheating in the whole solar plant.

2.2 Numerical model for two-phase flow

In this study, the boiling heat transfer coefficient is estimated via the correlation proposed by Gungor and Winterton [31]. The two-phase flow heat transfer process is divided into two components: a nucleate boiling contribution and a single-phase convection contribution for saturated water.

$$h_{2p} = Sh_{nb} + Eh_l \tag{1}$$

The factor S reflects the suppressed superheat amid the forced convection compared with the pool boiling, and it can be expressed as:

$$S = (1 + 1.15 \times 10^6 E^2 \,\mathrm{Re}_l^{1.17})^{-1} \tag{2}$$

where the Re_l is the Renold number of the liquid phase:

$$\mathrm{Re}_l = \frac{G(1-x)D_{in}}{\mu_l} \tag{3}$$

and G is the mass flux, kg/(m^2•s); x is the vapor quality, D_{in} is the inner diameter of the tube, m; μ_{l} is the dynamic viscosity of the working fluid, Pa•s.

Factor E represents the enhanced convection and higher velocity in the two-phase flow compared with the single-phase flow condition.

$$E = 1 + 24000 Bo^{1.16} + 1.37 X_{tt}^{-0.86} \tag{4}$$

where the Bo and X_{tt} are two dimensionless numbers that are called the boiling number and Martinelli number, respectively. They are expressed as:

$$Bo = \frac{q_{abs}}{G\left(h_g - h_l\right)} \tag{5}$$

$$X_{tt} = \left(\frac{\rho_g}{\rho_l}\right)^{0.5} \left(\frac{\mu_l}{\mu_g}\right)^{0.1} \left(\frac{1-x}{x}\right)^{0.9} \tag{6}$$

where q_{abs} is the thermal flux, W/m^2; ρ_{g} and ρ_{l} are the density of liquid and vapor phase, respectively, kg/m^3. The physical property parameters are calculated at the saturated state by the REFPROP 10.0 software.

For the nucleate boiling coefficient h_{nb}, it can be calculated as:

$$h_{nb} = 55 {p_r}^{0.12} (-\log_{10}^{p_r})^{-0.35} M^{-0.5} q_{abs}^{0.67} \tag{7}$$

where p_r is the ratio between the pressure in the flow tube and the critical pressure of the working fluid. M is the relative molecular mass of the working fluid, g/mol.

The single-phase forced convection flow in the tube is modeled with the Dittus-Boelter equation [32]:

$$h_l = 0.023 \left(\frac{\lambda_l}{D_{in}} \right) \mathrm{Re}_l^{0.8} \, \mathrm{Pr}_l^{0.4} \tag{8}$$

where the λ is the thermal conductivity, W/ (m•K); and Pr is the Prandtl number.

The pressure drop of the two-phase flow is sourced from the actual data of solar steam collectors [33]. For a two-phase flow, the pressure drop is defined as the product of the single-phase water flow and factor *R*.

$$\left(\frac{dp}{dl} \right)_{2p} = R \left(\frac{dp}{dl} \right)_l \tag{9}$$

with,

$$\left(\frac{dp}{dl} \right)_l = 0.316 \, \mathrm{Re}^{-0.25} \frac{1}{D_{in}} \frac{\rho}{2} v^2 \tag{10}$$

$$R = A + 3.43 x^{0.685} (1-x)^{0.24} \left(\frac{\rho_l}{\rho_g} \right)^{0.5} \left(\frac{\mu_g}{\mu_l} \right)^{0.22} \left(1 - \frac{\mu_g}{\mu_l} \right)^{0.89} Fr_l^{-0.47} We_l^{0.0334} \tag{11}$$

where $(dp/dl)_l$ is the pressure drop of the single-phase flow. The ρ and v are the liquid density and velocity, respectively. The parameters for factor *R* are expressed as follows:

$$A = (1-x)^2 + x^2 \left(\frac{\rho_l}{\rho_g} \cdot \frac{\xi_g}{\xi_l} \right)^{0.8} \tag{12}$$

$$Fr_l = \frac{G^2}{\rho^2 g D_{in}} \tag{13}$$

$$We_l = \frac{G^2 D_{in}}{\rho\gamma} \tag{14}$$

where g is the gravitational acceleration, m/s^2, γ is the surface tension, N/m.

2.3 Numerical model of the direct steam generation EFPC

A numerical model for the direct steam generation EFPC is established for the thermal performance and energy flow analysis. For this model, the energy equilibrium equations for the key components in the solar collector are formulated, thereby the thermal performance of the solar collector is deduced by the thermodynamic first law.

The thermal equilibrium equation for the glass cover is:

$$\alpha_{\text{gla}} I + h_{\text{r,abs-gla}}(T_{\text{abs}} - T_{\text{gla}}) = h_{\text{r,g-a}}(T_{\text{gla}} - T_{\text{a}}) + h_{\text{c,g-a}}(T_{\text{gla}} - T_{\text{a}}) \tag{15}$$

with,

$$h_{\text{r,abs-gla}} = \frac{\sigma(T_{\text{abs}}^2 + T_{\text{gla}}^2)(T_{\text{abs}} + T_{\text{gla}})}{\frac{1}{\varepsilon_{\text{abs}}} + \frac{1}{\varepsilon_{\text{gla}}} - 1} \tag{16}$$

$$h_{\text{r,gla-a}} = \frac{\varepsilon_{\text{g}}\sigma(T_{\text{gla}}^4 - T_{\text{sky}}^4)}{(T_{\text{gla}} - T_{\text{a}})} \tag{17}$$

$$T_{\text{sky}} = 0.0552 T_a^{1.5} \tag{18}$$

$$h_{\text{c,gla-a}} = 5.7 + 3.8 v_{\text{wind}} \tag{19}$$

where α_{gla} and ε_{gla} are the absorptivity and emissivity of the glass cover, respectively; ε_{abs} is the emissivity of the absorber plate; σ is the Stefan-Boltzmann constant, 5.67×10^{8} W/(m^2•K^4); $h_{\text{r,abs-gla}}$ is the radiant heat transfer coefficient between the glass cover and absorber plate; $h_{\text{r,gla-a}}$ and $h_{\text{c,gla-a}}$ are the radiant and convection heat transfer coefficient between the glass cover and ambient, respectively; T_{gla}, T_{a}, and T_{sky} are the temperature of the glass cover, ambient and sky, respectively.

The thermal equilibrium equation for the absorber plate is:

$$\tau_{\text{gla}}\alpha_{\text{abs}}I = h_{\text{r,abs-gla}}(T_{\text{abs}} - T_{\text{gla}}) + h_{\text{r,abs-b}}(T_{\text{abs}} - T_{\text{b}}) + h_{\text{cond,abs-tb}}(T_{\text{abs}} - T_{\text{tb}}) \tag{20}$$

with,

$$h_{\text{r,abs-b}} = \frac{\sigma(T_{\text{abs}}^2 + T_{\text{b}}^2)(T_{\text{abs}} + T_{\text{b}})}{\dfrac{1}{\varepsilon_{\text{abs}}} + \dfrac{1}{\varepsilon_{\text{b}}} - 1} \tag{21}$$

$$h_{\text{cond,abs-tb}} = \frac{\lambda_{\text{weld}} b}{r} \tag{22}$$

where $h_{\text{r,abs-b}}$ is the radiant heat transfer coefficient between the absorber plate and bottom plate; $h_{\text{cond,abs-tb}}$ is the conductivity heat transfer coefficient between the absorber plate and absorber tubes; ε_{b} is the emissivity of the bottom plate; λ_{weld}, b, and r are the thermal conductivity coefficient, average width and average thickness of the welding material, respectively; T_{abs}, T_{tb}, and T_{b} are the temperature of the absorber plate, absorber tube, and bottom plate, respectively.

The thermal equilibrium equation for the absorber tube is:

$$h_{\text{cond,abs-tb}}(T_{\text{abs}} - T_{\text{tb}}) = h_{\text{tb-f}}(T_{\text{tb}} - T_{\text{f}}) \tag{23}$$

with,

$$h_{\text{tb-f}} = \left(\ln\left(\frac{D_{\text{out}}}{D_{\text{in}}}\right) \bullet \frac{1}{2\pi\lambda_{\text{tb}} l_{\text{tb}}} + \frac{1}{h_{\text{2p,f}}} \right)^{-1} \tag{24}$$

where $h_{\text{tb-f}}$ is the heat transfer coefficient between absorber tubes and the HTF that is comprised of the heat conductivity of the absorber tube itself and the two-phase flow boiling heat transfer coefficient of the HTF; D_{out}, D_{in}, λ_{tb}, l_{tb} are the inner and outer diameter, thermal conductivity, and length of the absorber tubes; $h_{\text{2p,f}}$ is the two-phase heat transfer coefficient of the working fluid that can be calculated from the numerical model in the previous section. T_f is the fluid temperature that is considered constant during the phase change process.

The enthalpy of heat transfer fluid will rise by absorbing the heat from absorber tubes:

$$h_{\text{tb-f}}(T_{\text{tb}} - T_{\text{f}}) = H_{\text{out}} - H_{\text{in}} \tag{25}$$

where H_{out} and H_{in} are the enthalpy of the outlet and inlet HTF, respectively.

The thermal equilibrium equation for the back bottom plate is:

$$h_{\text{r,abs-b}}(T_{\text{abs}} - T_{\text{b}}) = h_{\text{r,b-grd}}(T_{\text{b}} - T_{\text{grd}}) + h_{\text{c,b-a}}(T_{\text{b}} - T_{\text{a}}) \tag{26}$$

with,

$$h_{\text{r,b-grd}} = \frac{\sigma(T_{\text{b}}^2 + T_{\text{grd}}^2)(T_{\text{b}} + T_{\text{grd}})}{\dfrac{1}{\varepsilon_{\text{grd}}} + \dfrac{1}{\varepsilon_{\text{b}}} - 1} \tag{27}$$

$$h_{\text{c,b-a}} = 5.7 + 3.8 v_{\text{wind}} \tag{28}$$

where $h_{r,b\text{-}grd}$ is the radiant heat transfer coefficient between the bottom plate and ground; $h_{c,b\text{-}a}$ is the convection heat transfer coefficient for the bottom plate and the ambient surrounding.

Due to each heat transfer coefficient for the above equations being closely related to the temperature of each component, the calculation process should be iterated until the results' accuracy are satisfied. The main calculation process is depicted in the flow chart in Fig. 2.

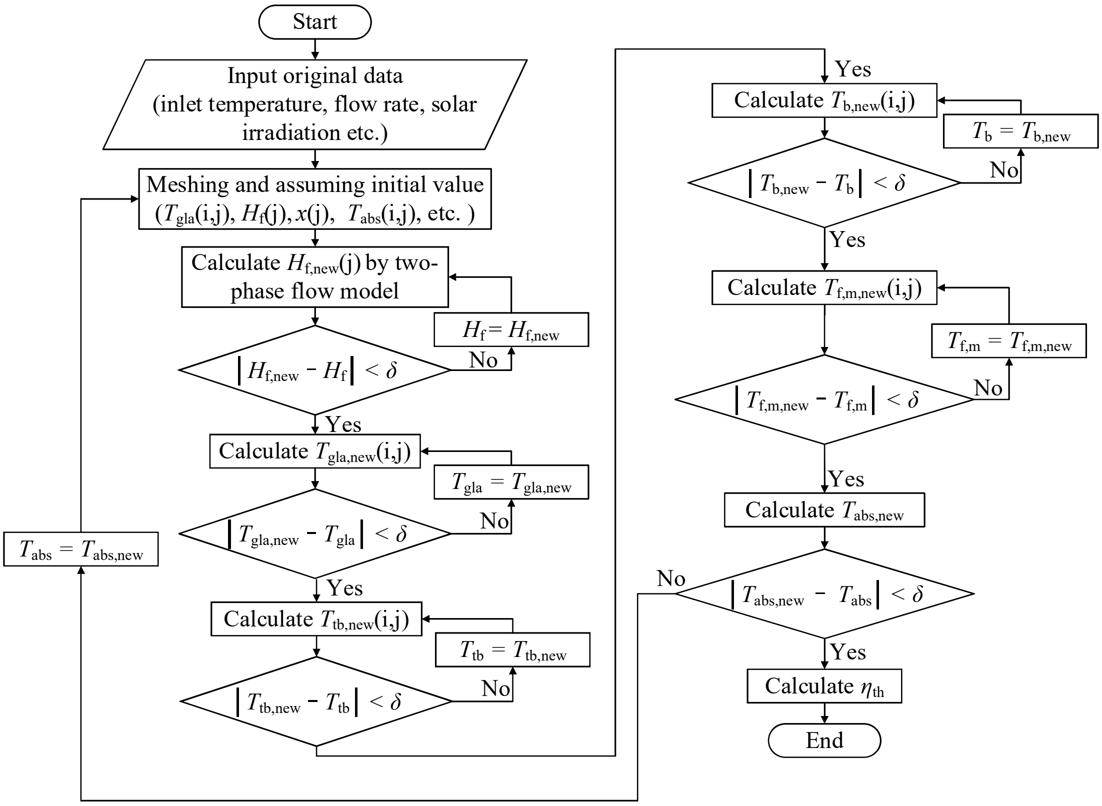

Fig. 2 The calculation process of the direct steam generation EFPC.

2.4 Experimental validation

To validate the precision of the above numerical model and demonstrate the superiority of this system, the thermal performance of the pressurization water mode test experiment is conducted via a medium-scale (50.96 m^2) EFPC platform comprised of 26 pieces of EFPC panels (the test rig in Fig. 3). The long-term experimental results are given in Fig. 4. It is observed that the simulation thermal efficiency curve agreed well with the experimental results. In light of the calculation method of the mean relative error (MRE) in Eq. (29) [34], the accuracy of this model is 1.80%. This deviation between the experimental and simulation results is mainly caused by the ideal spectrum characteristic of the simulation model and the measurement error of the experimental test.

$$MRE = \frac{\sum_{i=1}^{N} \left| X_{\text{exp}} - X_{\text{sim}} \right|}{\sum_{i=1}^{N} X_{\text{exp}}} \times 100\% \tag{29}$$

Fig. 3 The experiment platform of EFPC.

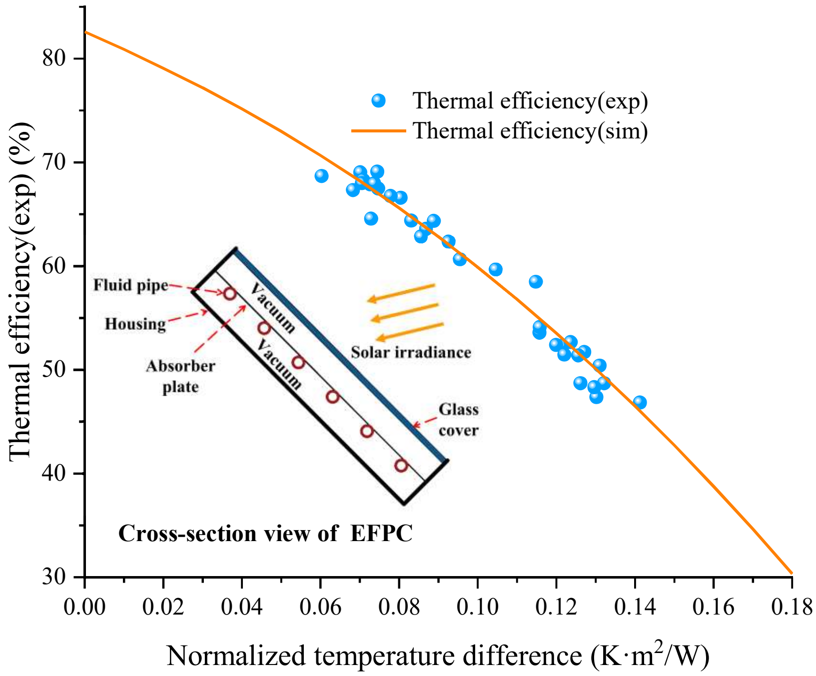

Fig. 4 The experimental validation of the EFPC.

The boiling heat transfer process is modeled based on the numerical model in [33, 35]. It is also validated via an experiment for boiling heat transfer in horizontal fluid pipes [36] (see Fig. 5). The simulation results are well-matched with the test values in all vapor quality ranges as depicted in Fig. 6. According to Eq. (29), the MRE of this model is 1.81%. This deviation between the experimental and simulation mainly results from the semi-empirical relationship used in the simulation model and the measurement error in the experiment process.

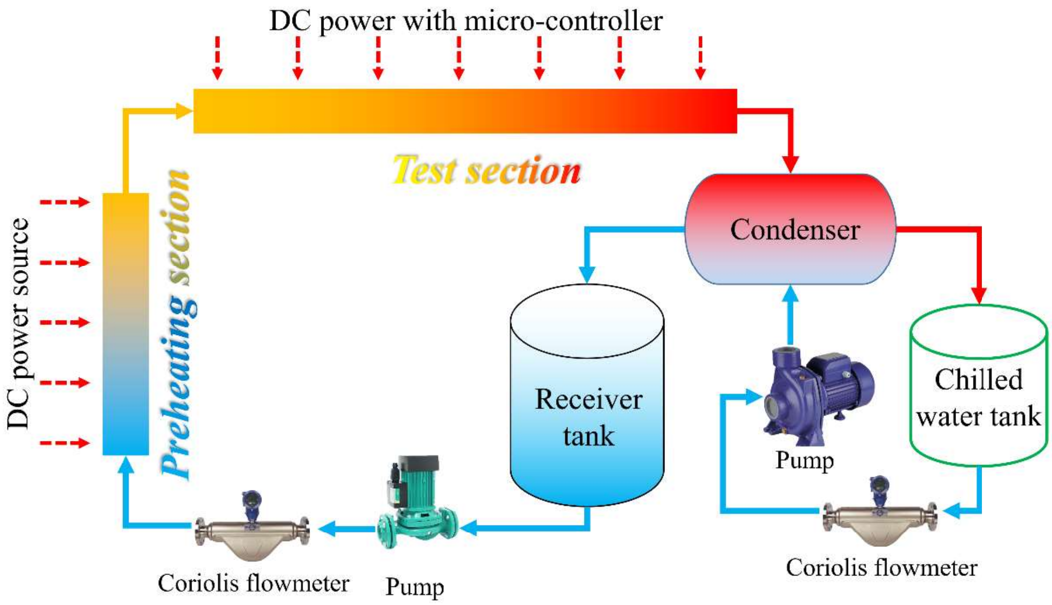

Fig. 5 The experimental test rig of the boiling heat transfer in horizontal tubes.

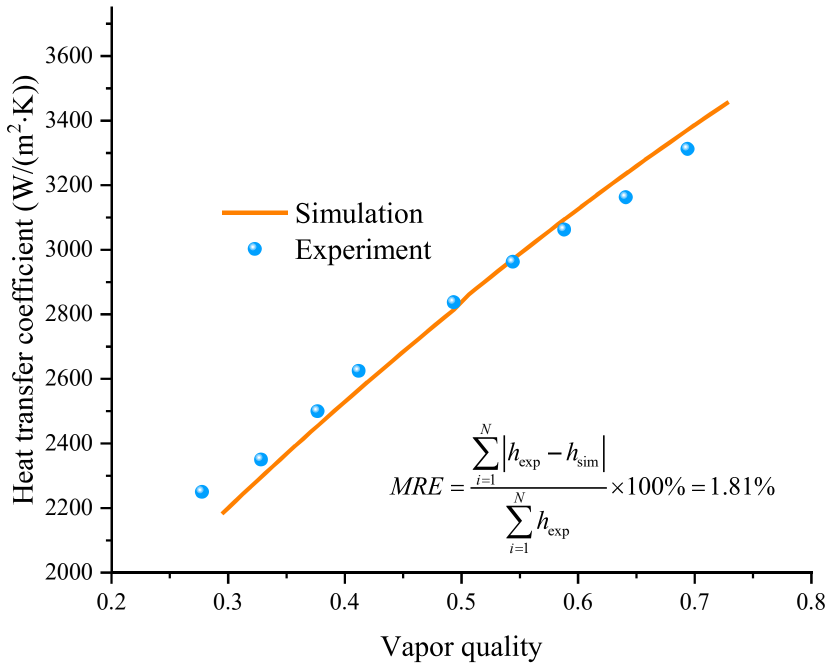

Fig. 6 The experimental validation of the numerical model for boiling heat transfer in horizontal tubes.

2.5 **Economic and environmental evaluation**

To evaluate the comprehensive performance of the system proposed in this paper, the economic and environment index are modeled for quantitative evaluation. The economic performance of this system is evaluated by the dynamic payback period P_{t} defined as Eq. (30).

$$\sum_{t=0}^{P_t}(CI-CO)_t \cdot (1+i_{\mathrm{c}})^{-t} = 0 \tag{30}$$

where CI and CO are the cash income and outcome, respectively. i_{c} is the benchmark yield for the system.

For the solar thermal and other devices, the initial equipment costs are calculated by [37]:

$$\begin{gathered} C_{\mathrm{eq}} = (1+\beta_{\mathrm{CF}})\sum_{k}(PEC_k \cdot FBM_k) \\ k \in \{\text{solar panels, flash vessel, and pump} \cdots\} \end{gathered} \tag{31}$$

where β_{CF} is the factor of the contingency fees, and the FBM_k is the bare module factor that considers the costs of transportation and installation. The PEC_k is the function of the cost of the k_{th} component of all scenarios, including the EFPC panels, flash vessel, pump, and so forth. It is the function of components and their installed capacity, i.e., $PEC_{\mathrm{k}} = f(k, CAP_{\mathrm{k}})$, and it is given in Table 1.

Table 1 Cost function of the main components.

Components	PEC_k	CAP_k type	Ref.
Solar thermal panels	$150\times CAP_{\mathrm{ST}}$	Aperture area (m^2)	\
Pump	$389\times\ln\left(\frac{CAP_{\mathrm{pump}}}{1000}\right)-283.15$	Flow rate (kg/h)	[38]
Flash vessel	$3955.3\times CAP_{\mathrm{vessel}}^{0.653}$	Volume (m^3)	[39]

Auxiliary boiler	$225.01 \times CAP_{\mathrm{boiler}}^{0.746}$	Power (kW)	[40]

Besides, the maintenance and operation cost is established as the function of the initial costs. It is set as 1.50% of the initial costs each year in the system lifespan.

The CO_2 emission reduction amount is adopted as the environmental evaluation index for this dual-mode system. It is defined as the CO_2 emission amount difference between a virtual system that assumes the energy supplied all by a natural gas boiler and this dual-mode EFPC system.

$$CER = \Delta Q_{\mathrm{ng}} \bullet f_{\mathrm{ng}} - Q_{pump} f_{ele} \tag{32}$$

where the ΔQ_{ng} refers to the natural gas reduction compared with the conventional gas boiler, Q_{pump} is the total electricity consumption of the solar plant, and the f_{ng} and f_{ele} is the CO_2 emission factor of natural gas which takes the value as 0.202 kg/kWh and 0.598 kg/kWh [41].

3. Results and discussion

To clearly show the superiority of the direct steam generation mode based on the EFPC, its thermal efficiency under the steady-state is investigated and compared with the pressurization water working mode. Then, the boiling heat transfer and the radiant thermal loss situation are also explored to explain. Finally, the internal energy flow relationships are presented for proving the above point of view.

3.1 Thermal efficiency analysis

The steady-state thermal performance of the two scenarios: direct steam generation mode and pressurization water mode are compared in this section. The boundary conditions for both scenarios are set at the same with the solar irradiance being 1000 W/m^2, the ambient temperature being 25 °C, and the wind velocity being 2 m/s. For the direct steam generation mode, the inlet HTF is under saturated condition, i.e., the dryness of HTF is 0.

From the perspective of the whole solar plant, the thermal efficiency curves are illustrated in Fig. 7. With this novel non-concentrating solar collector design, the thermal efficiency of the direct steam generation mode is about 10% higher than the pressurization water mode for the whole medium temperature range. At a typical steam generation temperature of 130 °C, the thermal efficiency of the direct steam generation mode reaches 70.19%. The reasons for the thermal efficiency promotion can be mainly ascribed to the following issues. Firstly, the thermal radiation losses are dramatically suppressed owing to the almost constant temperature in the working fluid phase change process of direct steam generation mode. However, the heat transfer process will deteriorate if the steam dryness rises to a much higher level. In this situation, the heat transfer process between the absorber tube and HTF will be close to the single-phase vapor. Secondly, the boiling heat transfer coefficient in the direct steam generation mode is much higher than the convection heat transfer coefficient of the pressurization water mode. These two aspects will be quantitatively described in the below section exhaustively.

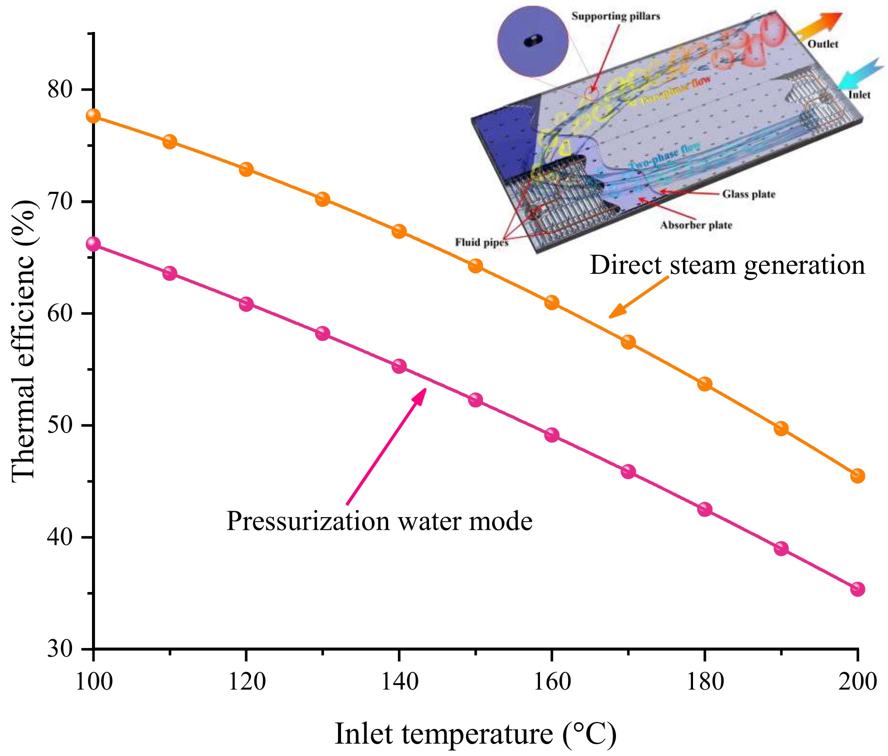

Fig. 7 The thermal performance of the direct steam generation and pressurization water EFPC plant.

Generally, the HTF (such as water, organic fluid, etc.) has a much larger latent heat storage capacity than sensible heat [32]. Hence, the higher thermal efficiency and using two-phase steam as HTF also has a huge mass flow and energy storage capacity saving potential. In the pressurization water mode, a storage tank is usually adopted as an energy storage device for a solar heating system. It should be designed at a certain size to prevent overheating of the solar plant and satisfy the requirement of the subsequent device. For the same storage capacity, energy storage in a steam flash vessel that uses latent heat as the thermal energy storage medium has less storage medium needed. For the regions that are facing severe water scarcity (such as west China and Africa which possess abundant solar resources), the HTF for the solar plant will lead to vast operating and maintenance costs. The direct steam generation-based EFPC solar plant will also release the water supply pressure there.

3.2 Heat transfer coefficient enhancement

The heat transfer coefficient between the HTF and absorber tube is quantitatively compared for the two scenarios in this section in terms of the solar panel array. A typical inlet temperature is selected at 150 °C and the other ambient parameters are the same as in Section 3.1.

The boiling heat transfer coefficient improved dramatically along with the solar panels' array while the nuances of the convection heat transfer coefficient in the pressurization water mode can be omitted (see Fig. 8). For the two-phase flow, along the flow direction of the HTF, the dryness of steam will rise progressively. Therefore, the boiling heat transfer coefficient for each panel is also varying with respect to the rising steam quality and pressure drop caused by the flow friction. For the pressurization water flow, the convection heat transfer coefficient will also increase owing to their thermodynamic properties (such as the specific capacity, thermal conductivity, density, etc.) will change concern with the operating temperature. The maximum heat transfer coefficient of the direct steam generation mode is over 10000 W/(m^2•K) which is almost an order of magnitude higher than the pressurization water mode.

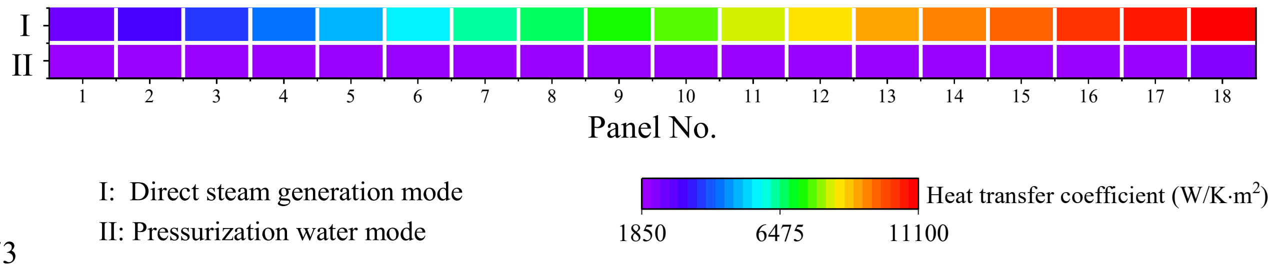

Fig. 8 The average heat transfer coefficient of each panel in the solar plant.

As the holistic thermal resistance network of EFPC is shown in Fig. 9, the direct steam generation mode alters the convection heat transfer thermal resistance essentially (red part). On average, the thermal resistance in this part has decreased by 66.34% with the steam generation implementation.

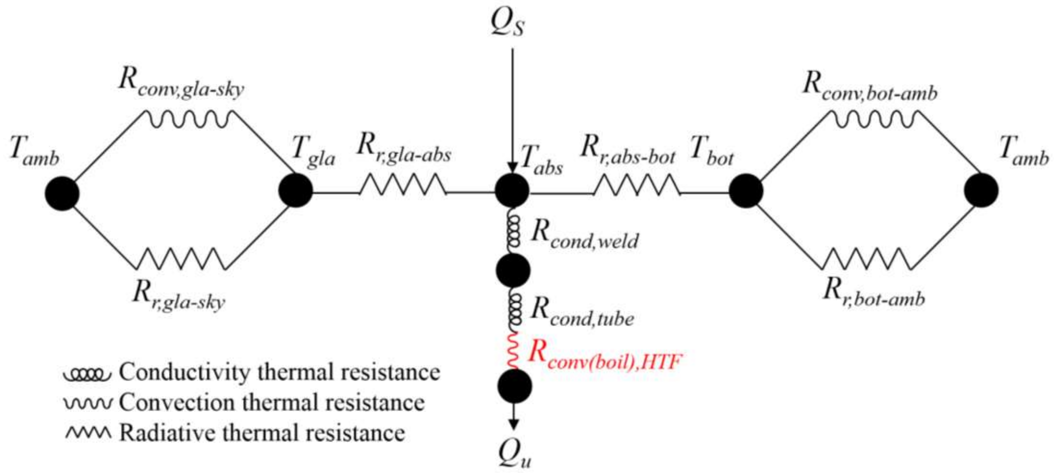

Fig. 9 Thermal resistance network of EFPC [27].

There are many other approaches for the thermal performance improvement of non-concentrating solar collectors. In terms of the heat transfer enhancement between the absorber tube and HTF in the flat plate solar collector, the most common ways that have attracted many researchers' attention are the micro-channel absorber plate [42], turbulence promotion structure [43], using nano-fluid [44] as HTF, or their combination [45, 46]. All of these technologies are aiming at enhancing the heat transfer coefficient and reducing the temperature difference between the absorber plate and HTF: The micro-channel plate makes the most use of the small hydraulic diameter for HTF [47]; The nano-fluid elevates the high thermal conductivity of HTF by dispersing special particles into it; The turbulence promotion structure adopts some inserts to the absorber tubes to generate the turbulence effect. In light of the convection heat transfer formula [32]: $h = Nu \cdot \lambda_w / D$, all these three approaches can increase the heat transfer coefficient, thereby increasing the thermal efficiency of the solar panel.

However, the heat transfer coefficient enhancement of all these methods is not in the same magnitude order as the boiling heat transfer, and the extra pump power consumption and maintenance of nano-fluid will lead to extra costs that may outweigh the extra energy gain [48]. Although some researchers use micro-channel collectors with boiling heat transfer [49], the HTF of their studies should be organic fluid but water. These HTF types (usually the organic fluids) are not easily obtainable and toxic for practical application. More importantly, the direct steam generation is much more useful in the industrial sectors that can’t be realized by the above approaches.

3.3 **Thermal loss for the solar plant**

The EFPC processes a high-vacuum internal environment to prevent heat conductivity and heat convection losses from the absorber plate. Thus, the main heat loss is the thermal radiative losses from the absorber plate to the environment through the glass plate (top side) and backplate (bottom side). The total heat losses from these two parts are presented in Fig. 10 in terms of each solar panel.

For the pressurization water mode EFPC-based solar plant, the thermal loss for each solar panel will increase along the flow direction. The reasons can be ascribed to the progressively increasing operating temperature of the absorber plate. Since the EFPC is highly vacuumed, the thermal radiant loss is the main heat loss form and it is related to the four powers of the absorber plate temperature conforming to Stefan-Boltzmann's law. The relatively lower average operating temperature of the direct steam generation mode leads to the thermal radiant loss has reached as low as 260 W/m^2 which is almost half of the pressurization water mode.

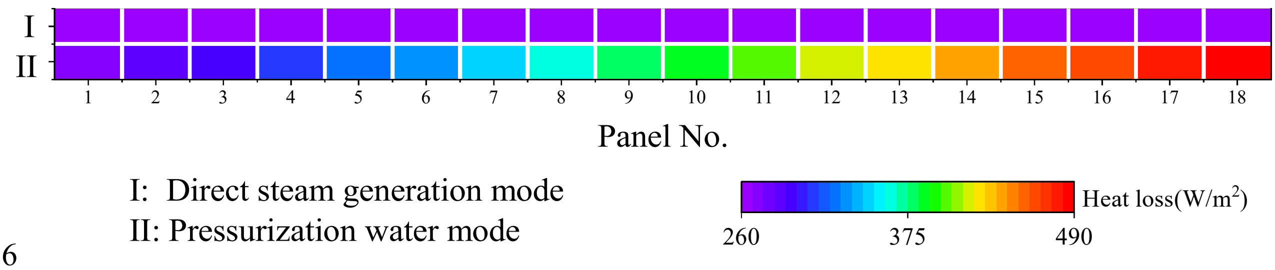

Fig. 10 The thermal loss distribution for each solar panel.

A representative solar panel among the EFPC system in these two working modes is chosen to exhibit the temperature distribution on the absorber plate (see Fig. 11). For the direct steam generation EFPC plant, the temperature of HTF is almost constant during the phase change process. Hence, the temperature of the absorber plate will also keep constant even amid the high-efficient solar harvesting process. The relatively low and uniform temperature distribution in the solar plant not only improves the highly efficient solar collection but also brings benefits for the low thermal stress in the absorber plate and tubes.

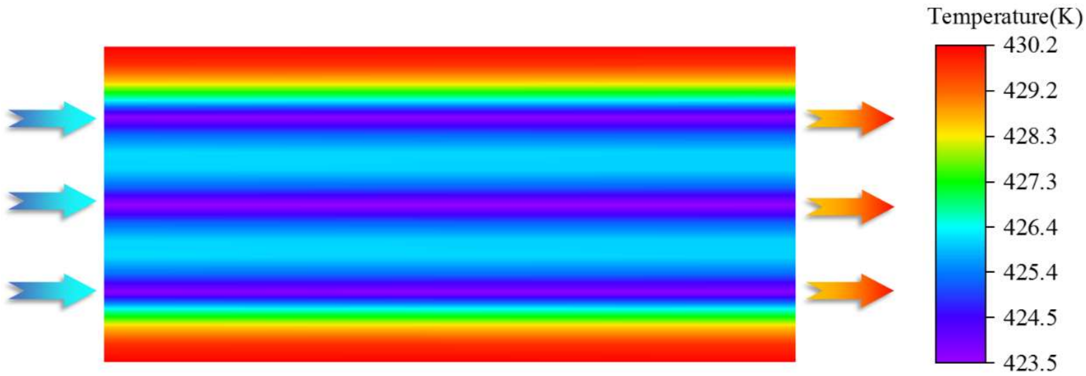

(a)

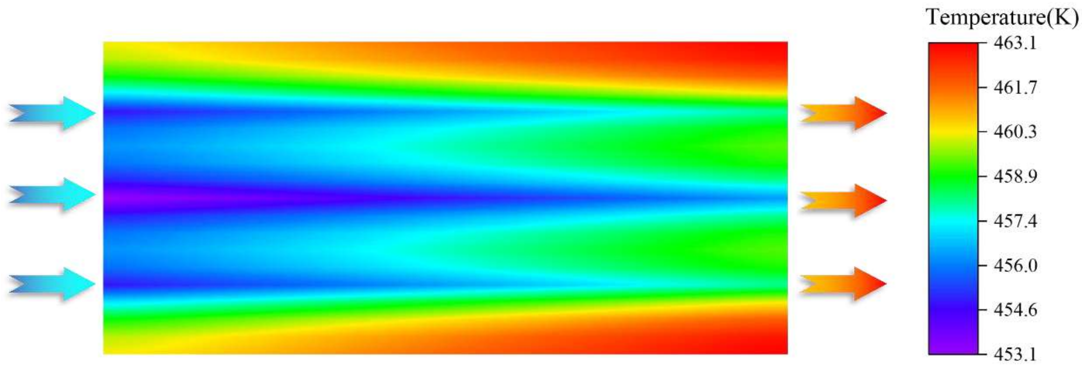

(b)

Fig. 11 The temperature distribution on a solar panel in (a) direct steam generation mode and (b) pressurization water operating mode.

3.4 Energy flow and transfer process

To clearly show the energy transfer and conversion process in the whole solar plant, the energy flow situations among each component of EFPC working in both the direct steam generation mode and pressurization water mode are presented in this section.

As depicted in Fig. 12, the solar irradiance of the whole solar plant will be converted into thermal energy in HTF through a series of processes. The glass cover and the absorber plate will lead to optical losses that are the same in both operation modes. The energy absorbed by the absorber plate will reemit to the glass cover (top side) and the backplate (bottom side). For the direct steam generation mode in Fig. 12 (a), the thermal radiative loss is much less than the pressurization water mode. Thus, more useful energy is obtained by the HTF.

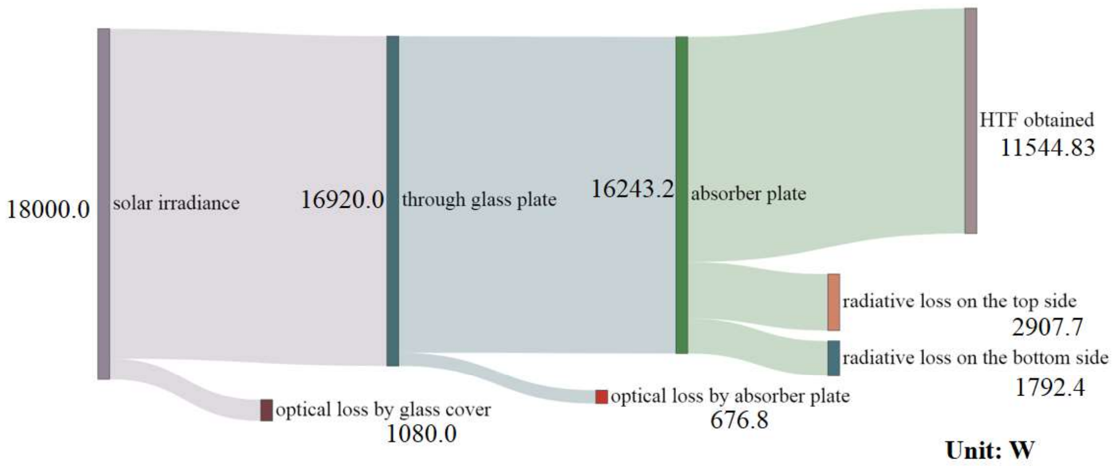

(a)

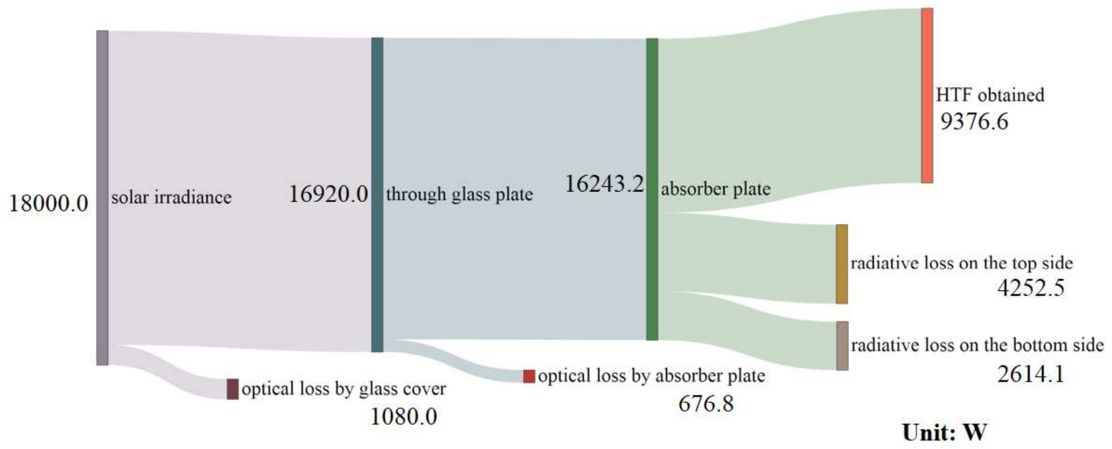

(b)

Fig. 12 The energy flow inside the EFPC panel of the (a) direct steam generation mode and (b) pressurization water mode.

4. Dual-mode solar thermal year-round utilization system

For the conventional solar thermal heating projects, there always exists a solar energy seasonal mismatch problem, i.e., the solar energy resource is abundant in the non-heating season but weak in the heating season. On the contrary, the space heating demand in the non-heating season is usually much lower than the heating season. If the conventional flat plate solar collector used for solar space heating continues to be put in use in the non-heating season, there will be a mass of low-temperature solar seasonal residual energy being useless. Hence, this seasonal mismatch issue in solar space heating projects will generally lead to the conventional non-concentrating solar collector being idle and the abundant solar energy is also wasted in the non-heating season [29]. The direct steam generation EFPC proposed in this paper can solve this seasonal mismatch problem by supplying the heating demand during the heating season preferentially while producing steam in the non-heating season. Thus, solar energy will be fully used for the whole year. In this section, the thermal performance and the comparison with state-of-art technology will be presented to show the superiority of this energy management strategy design.

4.1 Thermal performance

The energy gains for space heating in the heating season and steam generation in the non-heating season are presented in Fig. 13. According to the arrangement of most regions in east China, the heating season is from 15th Nov. to 15th Mar. next year and the rest period of the year is the non-heating season. For the space heating mode in the heating season, 50 °C hot water is produced for floor radiant heating. In the non-heating season, 130 °C low-pressure process steam is generated for industrial sectors. The thermal efficiency in the non-heating season is lower than the one during the heating season owing to the higher operating temperature but it is still around 50%. The year-round solar utilization efficiency for the dual-mode EFPC system is 52.59%. There is no extra device required and the only differences between these two working modes are the inlet temperature together with the operating pressure.

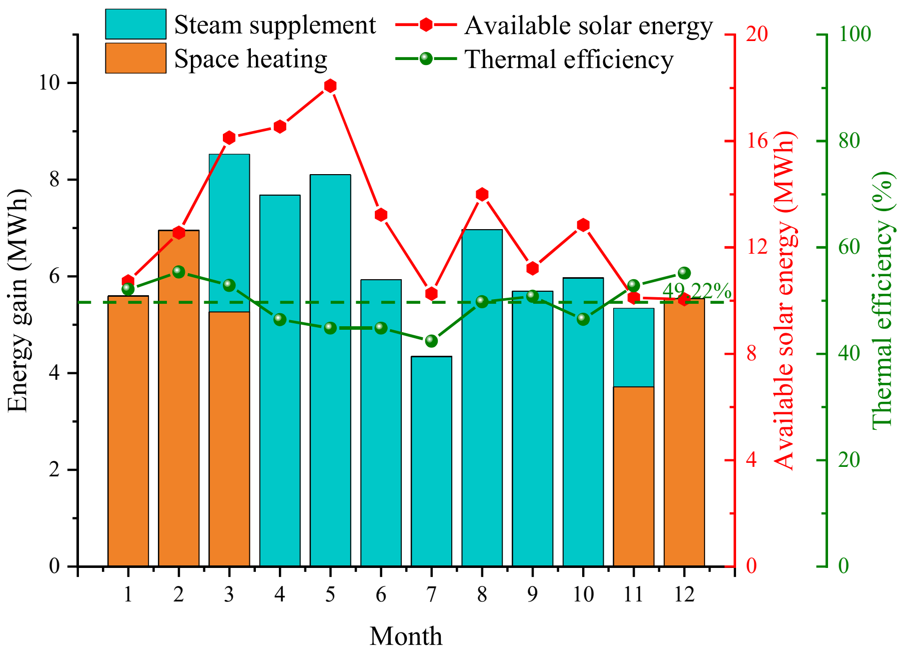

Fig. 13 The monthly energy gain of the dual-mode EFPC system.

4.2 Economic and environmental analysis

According to the evaluation model aforementioned, the economic and environmental performance of the dual-mode EFPC system is presented in this section. The economic evaluation uses the dynamic payback period as an index that takes the initial costs, maintenance and operation costs, and the temporal value of the fund into consideration. The yearly cash flow presented in Fig. 14 indicated that the payback period of this system is 9.02 years.

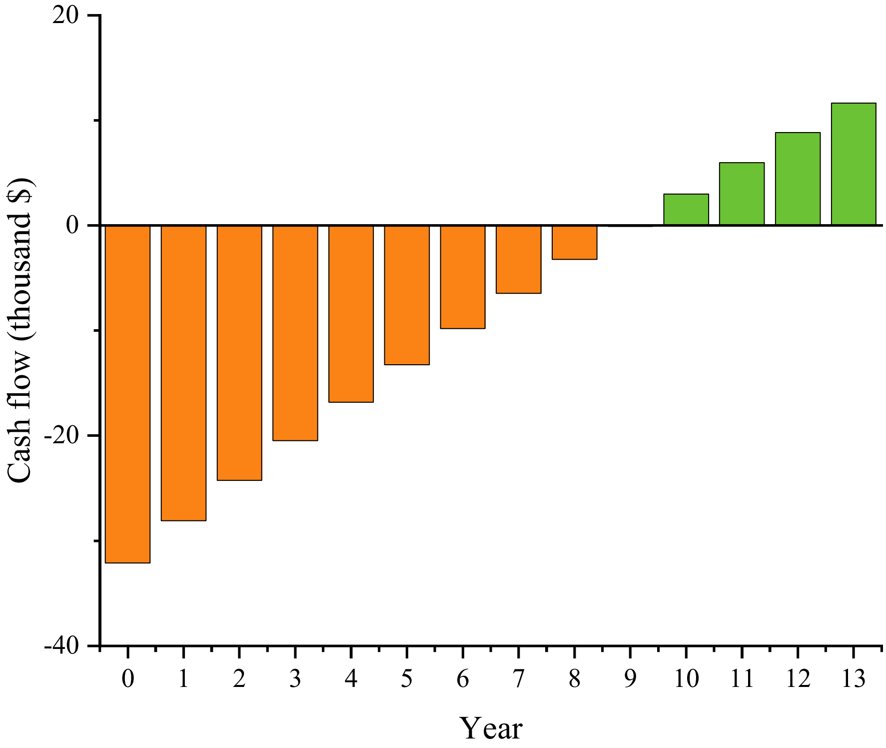

Fig. 14 The cash flow of the dual-mode EFPC system.

The environmental evaluation has considered the CO_2 reduction owing to the space heating and steam supplement from solar energy. The year-round electricity consumption by the pump is also taken into account as a carbon emission source of this system. The annual CO_2 reduction amount of the dual-mode EFPC system is 10142 kg.

4.3 **Comparison with the state-of-art technology**

To further demonstrate the superiority of the dual-mode EFPC system in this paper, an industrial factory in Jinan, China is selected as the target application object that needs space heating for the staff office building during the heating season and process steam for industrial products in the non-heating season. In the proposed solution in [50], an absorption-compression heat pump is adopted to elevate the temperature of the hot water produced by a solar plant (see Fig. 15).

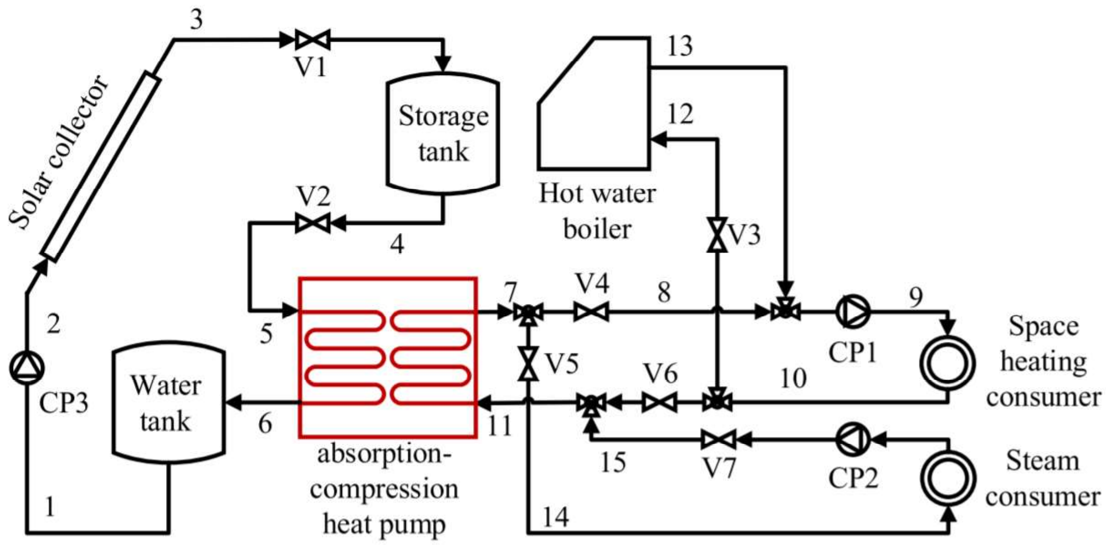

Fig. 15 The annual solar space heating and steam generation system [50].

The year-round thermal performance is dynamically simulated in accord with the same weather data and the same solar field area. The comparison results are given in Table 2. It can be observed that the energy gain for space heating in the heating season and the steam supplement in the non-heating season are both higher than the reference system. Although the reference system uses an absorption-compression heat pump to make the solar collector work under a relatively low temperature, the final year-round energy output for users is still not better than the dual-mode EFPC system in this paper. In addition, the heat pump will bring extra electricity consumption and a more complicated system configuration. Given the energy output results with the referred system are under the same solar field area, the dual-mode EFPC system can meet the same energy demand with less land occupation which is important in densely populated areas. Hence, the dual-mode EFPC system is more qualified for solar thermal energy utilization all year round.

Table 2 The comparison with the solar assistant heat pump system.

Items	EFPC system	Reference system [50]
Solar collector area/(m^2)	170	170
Tile angle/(°)	36.6	36.6
Heat pump capacity/(kW)	0	30
Design collection temperature in the heating/non-heating season/(°C)	50/130	30/85
Energy gain for space heating in the heating season/(MWh)	27.08	11.55
Energy gain for steam supplement in the non-heating season/(MWh)	49.03	40.17
Pay back period/(years)	9.02	10.10
CO_2 reduction/(kg)	10142	7187

5. Conclusions

In this paper, a direct steam generation solar system based on the non-concentrating solar collector is proposed. This system uses a novel evacuated flat plate solar collector that adopts a high-vacuum environment for high efficient solar harvesting and process steam generation. The shortcoming of the conventional solar steam generation system by concentrating solar collector is overcome and the knowledge gap of the high-efficient solar steam generation by the non-concentrating solar collector is filled. The heat transfer enhancement, thermal performance, and energy flow situation are detailed investigated and compared with the traditional solar plant. Furthermore, a dual-mode evacuated flat plate solar collector system based on the above research is also proposed to solve the solar seasonal mismatch problem. The main conclusions are drawn as follows.

1. The thermal efficiency of the direct steam generation model solar plant is around 10 percentage points (absolute value) higher than the pressurization water working mode in the medium temperature range. At a typical steam generation temperature of 130 °C, the thermal efficiency of the direct steam generation mode reaches 70.19%.
2. For the two working modes, the maximum heat transfer coefficient of the direct steam generation mode has reached over 10000 W/(m^2•K) which is much higher (with an order of magnitude enhancement) than the pressurization water working mode.
3. The relatively lower average operating temperature leads to the thermal radiant loss of the direct steam generation mode solar plant has reached as low as 260 W/m^2 which is almost half of the pressurization water mode. Moreover, it can not only promote solar energy harvesting to the HTF and eliminate the uneven distribution of the absorber plate.
4. The dual-mode evacuated flat plate solar plant can produce hot water for space heating in the heating season and generate steam in the non-heating season with a high solar year-round thermal efficiency. In comparison with the recent state-of-art work, the comprehensive performance of the dual-mode EFPC system in this paper is better for year-round solar energy utilization.

Acknowledgments

The study was sponsored by the National Natural Science Foundation of China (NSFC 52130601). The authors are grateful for support from the Joint research center for multi-energy complementation and conversion of the University of Science and Technology of China.

References

[1] S.H. Farjana, N. Huda, M.A.P. Mahmud, R. Saidur, Solar process heat in industrial systems - A global review, Renew Sust Energ Rev 82 (2018) 2270-2286.

[2] M. Feurhuber, A. Cattide, M. Magno, M. Miranda, R. Prieler, C. Hochenauer, Prediction of the fluid flow, heat transfer and inactivation of microorganism at medical devices in modern steam sterilizers using computational fluid dynamics, Appl Therm Eng 127 (2017) 1391-1403.

[3] A. Biglia, L. Comba, E. Fabrizio, P. Gay, D.R. Aimonino, Steam batch thermal processes in unsteady state conditions: Modelling and application to a case study in the food industry, Appl Therm Eng 118 (2017) 638-651.

[4] H.G. Pan, W.M. Zhong, Z.Y. Wang, G.X. Wang, Optimization of industrial boiler combustion control system based on genetic algorithm, Comput Electr Eng 70 (2018) 987-997.

[5] A. Vandermeulen, B. van der Heijde, L. Helsen, Controlling district heating and cooling networks to unlock flexibility: A review, Energy 151 (2018) 103-115.

[6] A. Frein, M. Motta, M. Berger, C. Zahler, Solar DSG plant for pharmaceutical industry in Jordan: Modelling, monitoring and optimization, Sol Energy 173 (2018) 362-376.

[7] A. Sanda, S.L. Moya, L. Valenzuela, Modelling and simulation tools for direct steam generation in parabolic-trough solar collectors: A review, Renew Sust Energ Rev 113 (2019).

[8] M. Palacio, A. Rincon, M. Carmona, Experimental comparative analysis of a flat plate solar collector with and without PCM, Sol Energy 206 (2020) 708-721.

[9] M.A. Sharafeldin, G. Grof, Efficiency of evacuated tube solar collector using WO3/Water nanofluid, Renew Energ 134 (2019) 453-460.

[10] M. Sheikholeslami, S.A. Farshad, Z. Ebrahimpour, Z. Said, Recent progress on flat plate solar collectors and photovoltaic systems in the presence of nanofluid: A review, J Clean Prod 293 (2021).

[11] L. Evangelisti, R.D. Vollaro, F. Asdrubali, Latest advances on solar thermal collectors: A comprehensive review, Renew Sust Energ Rev 114 (2019).

[12] J. Vestlund, M. Ronnelid, J.O. Dalenback, Thermal performance of gas-filled flat plate solar collectors, Sol Energy 83(6) (2009) 896-904.

[13] N. Benz, T. Beikircher, High efficiency evacuated flat-plate solar collector for process steam production, Sol Energy 65(2) (1999) 111-118.

[14] L.C. Xu, Z.H. Liu, S.F. Li, Z.X. Shao, N. Xia, Performance of solar mid-temperature evacuated tube collector for steam generation, Sol Energy 183 (2019) 162-172.

[15] Z.H. Liu, G.D. Tao, L. Lu, Q. Wang, A novel all-glass evacuated tubular solar steam generator with simplified CPC, Energ Convers Manage 86 (2014) 175-

185.

[16] M.A. Sabiha, R. Saidur, S. Mekhilef, O. Mahian, Progress and latest developments of evacuated tube solar collectors, Renew Sust Energ Rev 51 (2015) 1038-1054.

[17] K.E. Dami, R. Beltran-Chacon, S. Islas, D. Leal-Chavez, Numerical Simulation of Direct Solar Vapor Generation of Acetone for an Organic Rankine Cycle Using an Evacuated Tube Collector, J Sol Energ-T Asme 143(2) (2021).

[18] P. Mu, Z. Zhang, W. Bai, J.X. He, H.X. Sun, Z.Q. Zhu, W.D. Liang, A. Li, Superwetting Monolithic Hollow-Carbon-Nanotubes Aerogels with Hierarchically Nanoporous Structure for Efficient Solar Steam Generation, Adv Energy Mater 9(1) (2019).

[19] Y. Shi, R.Y. Li, Y. Jin, S.F. Zhuo, L. Shi, J. Chang, S. Hong, K.C. Ng, P. Wang, A 3D Photothermal Structure toward Improved Energy Efficiency in Solar Steam Generation, Joule 2(6) (2018) 1171-1186.

[20] O. Neumann, A.D. Neumann, E. Silva, C. Ayala-Orozco, S. Tian, P. Nordlander, N.J. Halas, Nanoparticle-Mediated, Light-Induced Phase Separations, Nano Lett 15(12) (2015) 7880-7885.

[21] H. Ghasemi, G. Ni, A.M. Marconnet, J. Loomis, S. Yerci, N. Miljkovic, G. Chen, Solar steam generation by heat localization, Nat Commun 5 (2014).

[22] L. Zhou, Y.L. Tan, D.X. Ji, B. Zhu, P. Zhang, J. Xu, Q.Q. Gan, Z.F. Yu, J. Zhu, Self-assembly of highly efficient, broadband plasmonic absorbers for solar steam generation, Sci Adv 2(4) (2016).

[23] X.Z. Hu, W.C. Xu, L. Zhou, Y.L. Tan, Y. Wang, S.N. Zhu, J. Zhu, Tailoring Graphene Oxide-Based Aerogels for Efficient Solar Steam Generation under One Sun, Adv Mater 29(5) (2017).

[24] H.R. Li, Y.R. He, Y.W. Hu, X.Z. Wang, Commercially Available Activated Carbon Fiber Felt Enables Efficient Solar Steam Generation, Acs Appl Mater Inter 10(11) (2018) 9362-9368.

[25] J.X. Chen, J. Feng, Z.W. Li, P.P. Xu, X.J. Wang, W.W. Yin, M.Z. Wang, X.W. Ge, Y.D. Yin, Space-Confined Seeded Growth of Black Silver Nanostructures for Solar Steam Generation, Nano Lett 19(1) (2019) 400-407.

[26] D. Gao, S. Zhong, X. Ren, T.H. Kwan, G. Pei, The energetic, exergetic, and mechanical comparison of two structurally optimized non-concentrating solar collectors for intermediate temperature applications, Renew Energ 184 (2022) 881-898.

[27] D. Gao, G. Gao, J. Cao, S. Zhong, X. Ren, Y.N. Dabwan, M. Hu, D. Jiao, T.H. Kwan, G. Pei, Experimental and numerical analysis of an efficiently optimized evacuated flat plate solar collector under medium temperature, Appl Energ 269 (2020).

[28] A. Ordaz-Flores, O. Garcia-Valladares, V.H. Gomez, Findings to improve the performance of a two-phase flat plate solar system, using acetone and methanol as working fluids, Sol Energy 86(4) (2012) 1089-1098.

[29] D. Gao, T.H. Kwan, M. Hu, G. Pei, The energy, exergy, and techno-economic analysis of a solar seasonal residual energy utilization system, Energy 248 (2022) 123626.
[30] M.T. Islam, N. Huda, A.B. Abdullah, R. Saidur, A comprehensive review of state-of-the-art concentrating solar power (CSP) technologies: Current status and research trends, Renew Sust Energ Rev 91 (2018) 987-1018.
[31] K.E. Gungor, R.H.S. Winterton, A General Correlation for Flow Boiling in Tubes and Annuli, Int J Heat Mass Tran 29(3) (1986) 351-358.
[32] S.K. Nellis Gregory, Heat transfer, Cambridge university press, 2008.
[33] M. Eck, W.D. Steinmann, Modelling and design of direct solar steam generating collector fields, J Sol Energ-T Asme 127(3) (2005) 371-380.
[34] X. Ren, J. Li, M. Hu, G. Pei, D. Jiao, X. Zhao, J. Ji, Feasibility of an innovative amorphous silicon photovoltaic/thermal system for medium temperature applications, Appl Energ 252 (2019) 113427.
[35] A.A. Hachicha, I. Rodriguez, C. Ghenai, Thermo-hydraulic analysis and numerical simulation of a parabolic trough solar collector for direct steam generation, Appl Energ 214 (2018) 152-165.
[36] J. Dirker, H. Scheepers, J.P. Meyer, The effect of circumferentially non-uniform heat flux on flow boiling heat transfer in a horizontal tube, Int J Heat Mass Tran 185 (2022).
[37] L.X. Li, H.L. Mu, N. Li, M. Li, Economic and environmental optimization for distributed energy resource systems coupled with district energy networks, Energy 109 (2016) 947-960.
[38] F. Calise, M.D. d'Accadia, A. Palombo, Transient analysis and energy optimization of solar heating and cooling systems in various configurations, Sol Energy 84(3) (2010) 432-449.
[39] V. Tulus, D. Boer, L.F. Cabeza, L. Jimenez, G. Guillen-Gosalbez, Enhanced thermal energy supply via central solar heating plants with seasonal storage: A multi-objective optimization approach, Appl Energ 181 (2016) 549-561.
[40] J.A.S. Richard Turton, Debangsu Bhattacharyya, Wallace B. Whiting, Analysis, synthesis and design of chemical processes, fifth edition ed., International Series in the Physical and Chemical Engineering Sciences, 2018.
[41] H. Yousefi, M.H. Ghodusinejad, Y. Noorollahi, GA/AHP-based optimal design of a hybrid CCHP system considering economy, energy and emission, Energy and Buildings 138 (2017) 309-317.
[42] G. Chen, Y. Tang, L.H. Duan, H. Tang, G.S. Zhong, Z.P. Wan, S.W. Zhang, T. Fu, Thermal performance enhancement of micro-grooved aluminum flat plate heat pipes applied in solar collectors, Renew Energ 146 (2020) 2234-2242.
[43] M. Fan, S.J. You, X.L. Gao, H. Zhang, B.J. Li, W.D. Zheng, L.Z. Sun, T.T. Zhou, A comparative study on the performance of liquid flat-plate solar collector with a new V-corrugated absorber, Energ Convers Manage 184 (2019) 235-248.
[44] M.A. Sharafeldin, G. Grof, O. Mahian, Experimental study on the performance

of a flat-plate collector using WO3/Water nanofluids, Energy 141 (2017) 2436-2444.

[45] L.S. Sundar, M.K. Singh, V. Punnaiah, A.C.M. Sousa, Experimental investigation of Al2O3/water nanofluids on the effectiveness of solar flat-plate collectors with and without twisted tape inserts, Renew Energ 119 (2018) 820-833.

[46] P.P. Thakur, T.S. Khapane, S.S. Sonawane, Comparative performance evaluation of fly ash-based hybrid nanofluids in microchannel-based direct absorption solar collector, J Therm Anal Calorim 143(2) (2021) 1713-1726.

[47] R.W. Moss, G.S.F. Shire, P. Henshall, P.C. Eames, F. Arya, T. Hyde, Optimal passage size for solar collector microchannel and tube-on-plate absorbers, Sol Energy 153 (2017) 718-731.

[48] M.H. Mousa, N. Miljkovic, K. Nawaz, Review of heat transfer enhancement techniques for single phase flows, Renew Sust Energ Rev 137 (2021).

[49] H.U. Helvaci, Z.A. Khan, Mathematical modelling and simulation of multiphase flow in a flat plate solar energy collector, Energ Convers Manage 106 (2015) 139-150.

[50] C. Liu, W. Han, Z. Wang, N. Zhang, Q. Kang, M. Liu, Proposal and assessment of a new solar space heating system by integrating an absorption-compression heat pump, Appl Energ 294 (2021) 116966.